Spatiotemporal morphological transitions in thin-layer electrodeposition: The Hecker effect

A. Kuhn and F. Argoul
Centre de Recherche Paul Pascal, Avenue Schweitzer, 33600 Pessac, France
(Received 26 October 1993)

We study the electrodeposition of zinc from zinc sulfate solutions in thin-layer cells. We report experimental demonstrations of the origin of the morphological transitions which have been shown in the literature to occur during the growth process. We discuss the type of migrating impurities which provoke such transitions and we check their actual implication in real experiments. We interpret their strong influence on both the microscopic and macroscopic textures of the deposit by a drastic modification of the interfacial reduction process.

PACS number(s): 81.10.Dn, 61.50.Cj, 64.60.Ak, 66.10.Ed

I. INTRODUCTION

In the past decade much effort [1,2] has been devoted to understanding nonequilibrium growth phenomena from both theoretical and experimental points of view. Well-known examples are viscous fingering [3–5], dielectric breakdown [6], growth of bacterial colonies [7], crystallization [8,9], and electrodeposition [10,11]. The latter is currently considered as a paradigm for these kinds of studies since a wide variety of structures can be obtained, depending on parameters such as the nature of the metallic salt, its concentration, the current density, and the geometry of the cell. With electrodeposition, one can explore different morphologies, for instance, dense radial, dendritic, and diffusion-limited-aggregation-(DLA) like fractal patterns [10–17].

During the growth of copper and zinc by electrodeposition, some striking morphological changes have been repeatedly observed by several authors [10–23] in the past, but some confusion, concerning the number and the origin of these transitions, remained. The original Hecker effect [18] has been described as a sudden change in color, roughness, and number of branches of the deposit at a certain distance between anode and cathode. The place where it occurs has been shown to scale with the size of the cell and generally values of one-half of the total distance between anode and cathode has been reported [18,19], but also values of one-fourth, three-fifths [20], 80%, and 90% [21] were found. Migrating acid [21] and impurity fronts [20] as well as fronts of high electrolyte concentration [21] or stability-driven branching transitions [19,23] have been proposed as explanations. In this paper we clarify, with new measurements, the different origins of these phenomena.

II. THE EXPERIMENTAL SETUP

The different setups are reported in detail elsewhere [24]. The cell mainly used in this work is composed of two parallel zinc wires (Zn 99.999% purchased from Aldrich) sandwiched between two glass plates and separated by a distance L of 2 to 10 cm. The width W of the cell is varied from 5 to 8 cm and the thickness D from 0.25 to 1 mm. The volume confined this way is filled with an aqueous solution of zinc sulfate (99% $ZnSO_4 \cdot 7H_2O$, ACS reagent, Aldrich) which has been treated, prior to use, by bubbling nitrogen through it for one hour. When required, different amounts of hydrogen peroxide (30% RP Normapur analytic reagent, Prolabo), sulfuric acid, and colored *p*H indicators are added to the solution.

Except for the circular geometry example, the whole set of experiments has been done under intentiostatic conditions with current densities j ranging from 10 to 100 mA cm^{-2}. The cell voltage signal is low-pass filtered and the amplified signal is digitized with 16 bit resolution and stored in a microcomputer. Pictures of the cell are grabbed by a three charge-coupled device (CCD) video camera and stored into a second microcomputer for further image analysis and characterization of the spatiotemporal evolution.

III. THE DIFFERENT TRANSITIONS

As mentioned in the Introduction, no fewer than five different morphological transitions have been reported in the literature [17–23]. Before considering each type of transition and elucidating the exact local mechanism which gives rise to it, we think it worth stressing the general character of these morphological changes. The fact that each transition invariably appears at a fixed percentage of the cathode-anode distance, independently of the size of the cell, is strong evidence that transport processes and, particularly in the high field regimes, migration play a crucial role in the selection of its position, as already discussed by Fleury and co-workers [20,25]. Nevertheless, most of the arguments that have been developed so far are open to criticism, since the role of the chemical species which are likely to induce these transitions has been neglected. Careful investigation of the interfacial chemical reactions was thus missing. We show subsequently that, in each case, the position and the nature of the morphological transition depend upon both the transport mechanism and the chemical species which can involuntarily be involved in the reduction mechanism. We discuss separately each transition, according to its occurrence in the growth process.

A. First transition: basic front transition

In a previous publication [26] we have shown that the generic structure of zinc electrodeposits is a dendritic monocrystal morphology, over a wide range of current density and concentration, as can be seen in Fig. 1(a). However, as soon as the electrolyte has come in contact with air, a modification of the former perfect structure can be observed. Figure 1(b) shows the influence of air aging on zinc electrodeposition morphology; in this case, the growth looks more disordered and spread, it also includes many defects, corresponding to the breaking of the hexagonal symmetry of the zinc metal. We have given, in Ref. [26], evidence for dissolved oxygen to be the prime cause for these modifications. The same effect has been obtained by the addition of small amounts of hydrogen peroxide [see Fig. 1(c)]. We concluded that molecular oxygen, by its reduction at the cathode, could form with the neighboring zinc ions a metal oxide which could block the most protuberant sites of the aggregate and therefore increase the sidebranching of the structure. In these experiments [Figs. 1(b) and 1(c)] we observe a sudden widening of the growth around 17% of the total length of the cell. If the amount of hydrogen peroxide is increased, the transition occurs earlier [7% in Fig. 1(d)] and finally disappears completely for higher peroxide concentrations as in Fig. 1(e). From Fig. 1(d) to Fig. 1(e) the ratio $r=[H_2O_2]/[Z_nSO_4]$ is varied from 0.02 to 0.1; the adsorption of oxygen completely inhibits the sidebranchings and gives a more compact, "dense" [17] morphology, where the local hexagonal symmetry is strongly disturbed. In almost all previous experiments reported in the literature, no oxygen purification of the electrolyte has been mentioned, while dissolved oxygen should be the first fundamental impurity to look for.

Let us now discuss the chemical mechanism, involving molecular oxygen, that is likely to produce the first Hecker transition. In "oxygen free" aqueous zinc sulfate solutions, two global reduction mechanisms have been shown to compete [24,27,28]; on the one hand, the reduction of zinc cations:

$$Zn^{2+}+2e^{-}\rightarrow Zn \tag{1}$$

and on the other hand, the reduction of protons:

$$2H^{+}+2e^{-}\rightarrow H_2 . \tag{2}$$

With oxygen, a third interfacial reduction mechanism has to be taken into account:

$$O_2+4e^{-}\rightarrow 2O^{2-} . \tag{3}$$

Moreover, as already argued in a previous publication [24] to interpret rhythmic growth dynamics in zinc electrodeposition, the confined thickness of the cells which is used to approximate quasi-two-dimensional conditions can favor some reduction mechanisms which would otherwise be inhibited by kinetic criteria. In particular, as soon as the current is switched on across the cell, in the induction period, a rapid depletion of zinc cations in the neighborhood of the cathode occurs and the flow of zinc

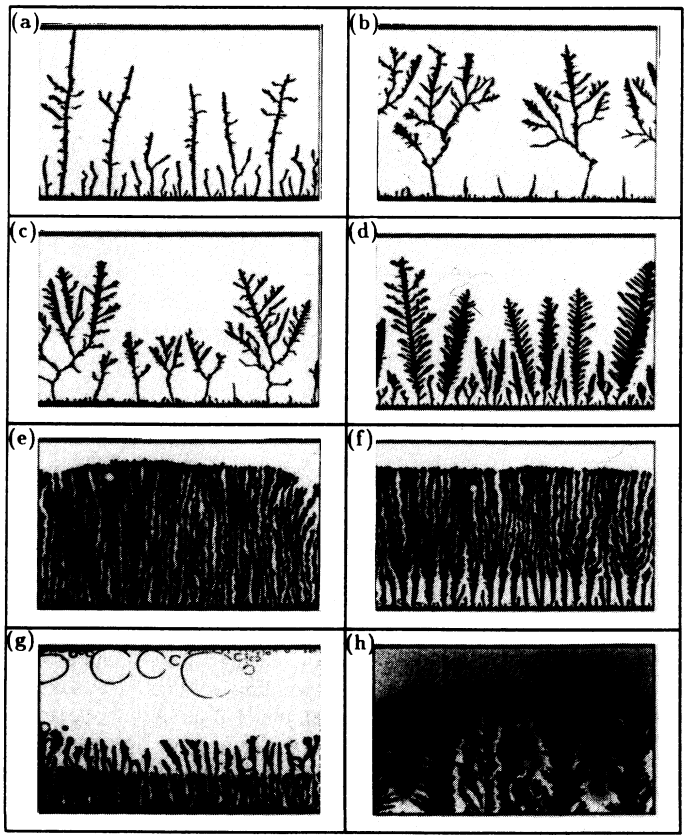

FIG. 1. Influence of the oxygen content and the acidity on the first morphological transition in thin-layer electrodeposition of zinc. The geometrical characteristics of the cell are width $W=5$ cm, length $L=2$ cm, and depth $D=0.25$ mm. The electrolyte is, except when otherwise mentioned, a $0.03M$ solution of $ZnSO_4$ with its normal pH and the current density is adjusted to 20 mA cm^{-2}. (a) The electrolyte has been purified by bubbling nitrogen through it for one hour; (b) without nitrogen purification; (c) after nitrogen purification, a proportion $r=[H_2O_2]/[ZnSO_4]=0.015$ of hydrogen peroxide has been added; (d) same as (c) with $r=0.02$; (e) same as (c) with $r=0.1$; (f) same as (e) with a pH adjustment to 2.7 by addition of sulfuric acid; (g) we have replaced the zinc anode by a silver anode, $r=0.1$, $[ZnSO_4]=0.03M$, and the current density j has been increased to 60 mA cm^{-2} to minimize the convective perturbation of the growth by the bubbles which are produced at the anode; (h) same as (f) with a few drops of pH indicator bromocresolpurple ($pK_a=6$): enlargement of the tips after the transition; the darker zone corresponds to the purple (basic) color of the indicator.

cations arriving by migration on the cathode becomes rapidly insufficient to supply the requested total current and consequently the reduction of protons increases. This leads to the emergence of a set of sharp spikes on the original flat electrode, as can be seen in Fig. 1(a). This morphology could be maintained across the whole cell if the protons were reproduced at the anode at the same rate as they are consumed at the cathode. This is not the case for a zinc anode, because no water oxidation occurs. Therefore the protons which migrate towards the cathode leave behind them a zone of higher pH (more basic; from which the term "basic front") which progressively invades the cell. When this "basic front" meets the growth, the reduction mechanism changes and, at that time, if molecular oxygen is present, its reduced form (O^{2-}) can no longer be recombined with protons to restore H_2O molecules but can lead to a drastic modification of the morphology by the process $Zn^{2+}+O^{2-}\rightarrow ZnO$, because zinc oxide is not reducible under these conditions. If the solution is free of oxygen, zinc and zinc hydroxide are both reduced when protons are lacking. The modification of the morphology is then hardly visible, indeed quite imperceptible as in Fig. 1(a), but we can guess that beyond 20% of the cathode-anode distance, the sidebranchings seem to be expanded.

Let us check now with crude arguments the position of this first transition. The basic front is expected, as far as migration can be considered as the predominant large scale transport process, to drift towards the cathode with a speed V_{BF} which depends on the mobility of the protons μ_{pr}: $\langle V_{BF}\rangle=\mu_{pr}\langle E\rangle$ where $\langle E\rangle$ is the global field across the cell. On the other hand, one can reasonably assume, in accordance with Fleury, Rosso, and Chazalviel [20], that the mean growth velocity of the deposit is strictly fitted to the velocity of the anions, being rejected from the cathode:

$$\langle V_{\text{growth}}\rangle=\mu_{an}\langle E\rangle\ . \tag{4}$$

A straightforward calculation leads to the results

$$\tau=\frac{\mu_{an}}{\mu_{an}+\mu_{pr}}\sim 19\% \tag{5}$$

for the relative position of the transition [20], in good agreement with our observations in Fig. 1.

Finally, one can explain the progressive disappearance of this transition from Fig. 1(c) to Fig. 1(e): the percentage of oxygen being increased, the proportion of protons is no longer adequate for capturing all the oxide ions and canceling their effect on the morphology. This statement has been verified by artificially increasing the initial concentration of protons of the solution used in Fig. 1(e). The result is reported in Fig. 1(f) where the deposition has been performed for pH=2.7, under otherwise identical experimental conditions; again, as long as the basic front does not meet the growth, the protons can inhibit the influence of oxygen upon the morphology.

The time evolution of the voltage of the electrochemical cell can provide additional information for the dynamical characterization of the growth process and therefore help in the detection of the transition in time. The voltage signal shows in general a decreasing tendency which reflects the average diminution of the electrolyte volume which has not yet been invaded by the deposit. In Fig. 2(a), we have focused on three different experiments, corresponding to Figs. 1(a), 1(e), and 1(f). When the growth morphology is made of dendritic monocrystals, i.e., when the electrolyte has been cleaned of any impurity as in Fig. 1(a), the voltage signal versus time undergoes an accelerated decrease, as can be seen on the dashed-dotted curve 1a. The negative curvature of the voltage curve 1a reflects the selection process that takes place between the dendrites in the cell. One of the initial dendrites, emerging from the cathode when current is switched on, overpasses the other ones. During this competition, some dendrites progressively slow down and the foremost dendrite grows faster and faster. Let us define

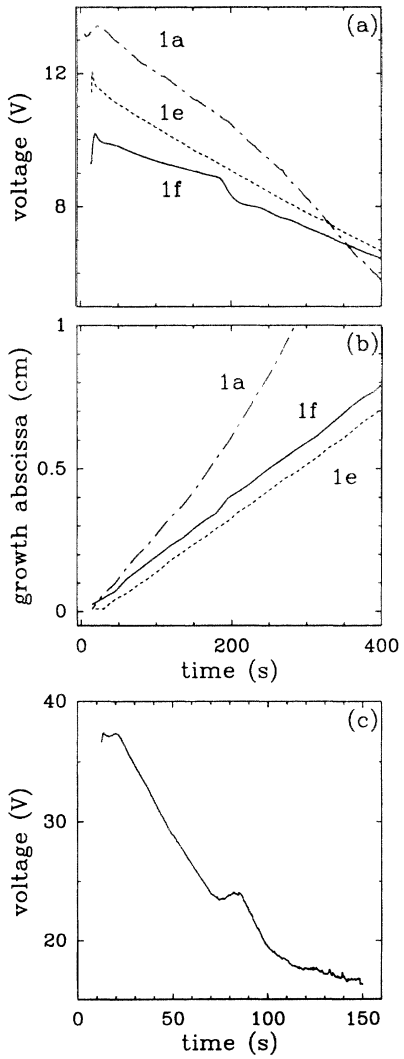

FIG. 2. (a) Temporal evolutions of the voltage (anode versus cathode arbitrary units) corresponding to Figs. 1(a) (dashed-dotted curve), 1(e) (dotted curve), and 1(f) (plain curve), respectively; (b) temporal evolutions of the growth abscissa corresponding to Figs. 1(a) (dashed-dotted curve), 1(e) (dotted curve), and 1(f) (plain curve), respectively; (c) temporal evolution of the voltage corresponding to 1(g).

the growth abscissa as the distance of the foremost branch of the growth from the original cathode. We show in curve 1*a* of Fig. 2(b) the evolution of the growth abscissa corresponding to curve 1*a* of Fig. 2(a); it confirms our interpretation of the voltage signal. On the other hand, when the growth morphology is dense as in Fig. 1(e), the voltage signal is rather linear [curve 1*e* of Fig. 2(a)] and this coincides with a constant growth velocity which can be deduced from curve 1*e* of Fig. 2(b).

Let us focus on Fig. 1(f), where the Hecker transition takes place around 20% of the cell. We observe at $t=200$ s a sudden decrease of the voltage curve 1*f* in Fig. 2(a) which is related to the spreading of the deposit towards a denser morphology. This sudden enhancement of the conductivity can be interpreted by the increase of the area of conducting material. This sharp variation of the voltage can also be seen on the temporal evolution of the growth abscissa [curve 1*f* of Fig. 2(b)]. We notice moreover that the growth velocity does not change noticeably before and after the small jump of the growth abscissa around 200 s. This confirms the validity of Eq. (4) when all the branches grow at the same speed (no selection process occurs).

To take advantage of our interpretation of this Hecker transition in terms of a basic front migrating from the anode towards the cathode, we show in Fig. 1(g) that the reverse transition can also be generated. Starting from a dense, "oxygen spoiled" morphology as in Fig. 1(e), we replace in Fig. 1(g) the zinc anode by a silver anode, where we know that the oxidation of water leads to oxygen formation and proton release at lower voltages. As a consequence, a higher proton concentration zone is created at the anode and starts to migrate towards the cathode. When this acid front meets the growth, the former disordered structure turns to well-ordered dendritic growth. This transition is evidenced in the cell voltage evolution, as shown in Fig. 2(c), and this time, the sudden bump in the voltage evolution reflects the sparser structure of the deposit which follows [in contrast to Fig. 2(a)]. Let us note that this transition arrives three times earlier because we have been obliged to multiply the current density by a factor of 3 to minimize the convective mixing of the electrolyte by the bubbles which are produced at the anode.

Another qualitative argument for a *p*H change during the experiment is the observation that, up to 20% of the cell length, small hydrogen bubbles are formed between the growing branches, whereas, at higher percentages, bubbles can no longer be detected, because the concentration of reducible protons has diminished. For the same reason, potential oscillations in zinc electrodeposition, which have been shown recently [24] to be related to competing proton reduction, cease in general around 20% of the growth evolution.

Finally, we can confirm the occurrence of a basic front by using *p*H colored indicators. As compared to the characterization by Melrose, Hibbert, and Ball of an acid front in the electrodeposition of copper [21], the situation happens to be a little trickier. We discuss here the artifice that we have devised for visualizing this basic front. Since the electrolyte is expected to become more basic during the electrodeposition process, we must choose an indicator that will be in its acid form when the experiment starts, i.e., for typical values of *p*H5.4±0.2, which corresponds to pure zinc sulfate in water. Therefore, with an indicator whose pK_a is higher than 6, we are sure that it will be in its acid form at the beginning and we can hope its color changes during the experiment. Moreover, its pK_a must not be too far from 5 because the variation of $[H_3O^+]$ is likely to be less than one order of magnitude in the basic front coming from the anode since zinc hydroxide would otherwise precipitate everywhere in the cell. In particular, if we take an indicator such as the bromocresol purple ($pK_a=6$), as shown in Fig. 1(h), we can only detect a local increase of the *p*H very close to the tip of the branches but no migrating basic front can be visualized. Figure 1(h) is nevertheless very instructive since it shows that, in a close neighborhood of the tips, the *p*H can reach quasineutrality, while inside the bulk it remains close to 6. This shows that the visualization of the basic front is rather difficult if one starts from simple zinc sulfate solutions, since generally two units of *p*H are necessary to clearly distinguish the acid color from the basic color of the indicator and it explains also the lack of such evidence in the literature. To circumvent this intrinsic limitation of *p*H indicators, we have adjusted the initial value of the *p*H to a lower value (around 3), assuming that the basic form of the front would still be around 6. We have then chosen bromocresolgreen ($pK_a=4.6$) as colored *p*H indicator. The result is shown in Fig. 3 where the basic front is clearly detected for different stages of the growth. After image processing and averaging the longitudinal sections of the cell, we get the type of profiles which are reported in Fig. 4. The leftmost part of Fig. 4(a) corresponds to the anodic side. From profile (1)

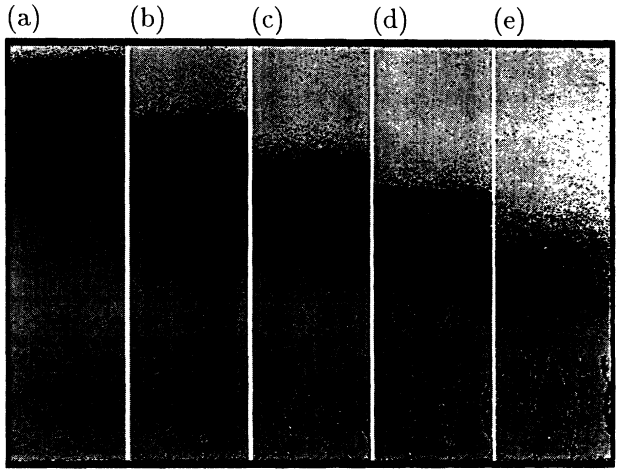

FIG. 3. Detection of the basic front with *p*H indicator bromocresolgreen ($pK_a=4.6$), $[ZnSO_4]=0.1M$, $j=60$ mA/cm^2, the *p*H has been adjusted to 3.2 by the addition of sulfuric acid. The distance L between anode and cathode is 5 cm. (a) $t=40$ s; (b) $t=120$ s; (c) $t=200$ s; (d) $t=280$ s; (e) $t=360$ s. Let us remark that as the growth evolves, the initial dark front which emerges from the anode (a) is getting wider and wider by diffusion process.

to profile (2) a sharp step forms, which corresponds locally to the increase of the *p*H above 5, since the protons escape first from this zone by migration towards the cathode. Meanwhile, the cathodic deposit [rightmost part of Fig. 4(a)] drifts more slowly towards the anode. Let us notice a small bump on the leading edge of the step of profile (2), which is moving slower than the basic front as time evolves. This bump limits a zone close to the anode where the *p*H does not seem to evolve much during the growth, since on profile (5), a quasiplateau forms in front of the anode. We have shown recently [29] that this plateau is the result of a convective instability of the fluid, driven by the local concentration gradients which are produced at the anode and at the cathode separately. We will show in the section devoted to the third transition that this anodic convecting zone, when it meets the growth, can also give rise to a morphological change.

By plotting the basic front position and the growth abscissa versus time in Fig. 4(b), we compute their average velocities: $v_{BF} \sim 150$ μm/s and $v_{growth} \sim 37$ μm/s and check that their ratio (~ 4) is close to the prediction given by the assumption of Fleury, Rosso, and Chazalviel [20], $v_{proton}/v_{anions} = v_{BF}/v_{growth} \sim 4.3$. Again the migrative character of the transport processes that determine the location of the Hecker transition is demonstrated in Fig. 4(c) where the velocity of the basic front is shown to vary linearly with the current density.

If one tries to generalize this interpretation of the Hecker transition to circular cell geometry with a central pointlike cathode, one has to take into account the fact that the electric field is now inversely proportional to the distance from the center of the cell. If we assume, as in Ref. [21], that the circular symmetry is preserved during the growth, we recover the following expression:

$$\tau = \frac{R(\text{Hecker})}{R(\text{anode})} = \left| \frac{\mu_{an}}{\mu_{an}+\mu_{pr}} \right|^{1/2} \quad (6)$$

for the relative radius of the transition. For sulfate anions and protons, this formula gives a value of τ around 43%. Figure 5 illustrates the circular configuration; straight dendrites emerge from the pointlike central cathode and meet the basic front coming from the anode at about 50% of the whole cell. The slight discrepancy with the prediction of Eq. (6) can be interpreted by some distortion of the assumed circular envelope of the structure before the transition since in that case the dendrites are not growing very dense. Let us note that the fact that the basic front transition (and generally most of the transitions) appears at different locations in circular and linear cells must have surely been a supplementary source of confusion for the interpretation of the Hecker effect. As for the parallel geometry, this basic front gives rise to a denser texture of the deposit, revealing the pollution of the electrolyte by dissolved oxygen. Finally, let us stress the fact that this transition is quite generic and does not depend on the initial morphology of the deposit, but rather on the presence of oxy-

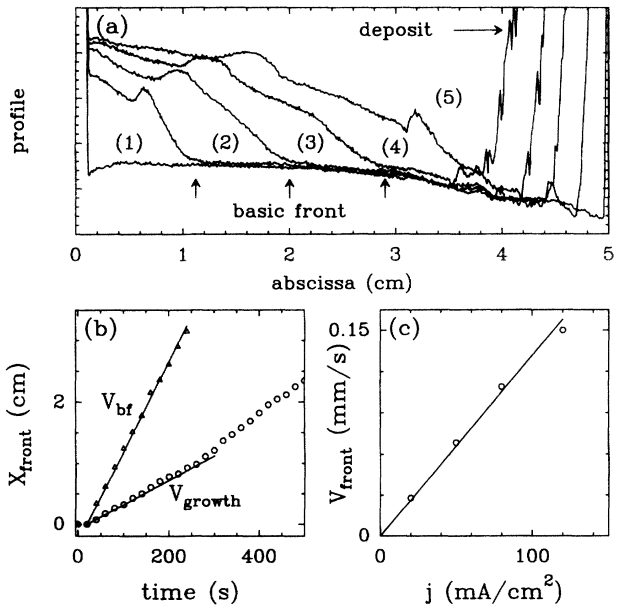

FIG. 4. (a) Averaged intensity profiles computed from longitudinal sections of the cell at successive times (1) $t = 60$ s, (2) $t = 120$ s, (3) $t = 180$ s, (4) $t = 240$ s, (5) $t = 300$ s through the electrolytic cell where a *p*H indicator (bromocresolgreen) has been added to visualize the basic front. The position of the anode is set to the origin while the cathode is positioned at $x = 5$ cm, $[ZnSO_4] = 0.1M$, $j = 120$ mA/cm^2, the *p*H has been adjusted to 2.9 by the addition of sulfuric acid. (b) Plots of the abscissa of the growth (○) and the basic front position (△) versus time as computed from the profiles of intensity reported in (a). The two lines V_{BF} and V_{growth} correspond to a linear fit of the data before the Hecker transition and give, respectively, the velocities $V_{BF} \sim 150$ μm/s for the basic front and $V_{growth} \sim 37$ μm/s for the growth. (c) Evolution of the velocity of the basic front versus the current density.

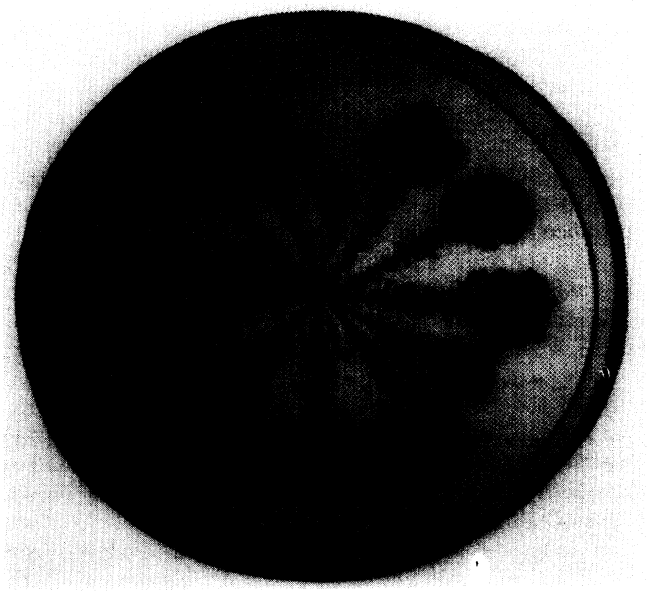

FIG. 5. The basic front transition in circular geometry. The diameter of the cell is 10 cm and its depth is 0.05 mm, $[ZnSO_4] = 0.05M$, $r = [H_2O_2]/[ZnSO_4] = 0.015$, *p*H = 2.7. The experiment is run under potentiostatic conditions with a global voltage $U = 5$ V.

gen, inadvertently dissolved inside the electrolyte, as has been the case in most of the quasi-two-dimensional experiments which have been carried out in the past.

B. Second transition: impurity transition

A second kind of transition, which occurs around 50–60 % of the cell in parallel geometry, has been reported by several authors [21,22]. Within the framework of the arguments that have been worked out in the preceding section, in particular the vanishing of chemical species (such as protons) which can cause a morphological change of the deposit, a 50–60 % transition is likely to be related to cationic impurities whose mobility is quite close to, or smaller than, the mobility of the anion. The species which are frequently included in aqueous electrolytes and which can perturb the electrodeposition process are alkali metal cations. In very recent publications [30,31], we have demonstrated the significant influence of these ions on the macroscopic and microscopic texture of the growth. In Figs. 6(a)–6(c), an increasing amount of sodium sulfate has been added to the zinc sulfate solution. The drastic modification of the morphology from Fig. 6(a) to Fig. 6(b), where only a 10^{-4} M concentration of sodium ions has been added to the initial zinc sulfate solution, illustrates the strong influence of these ions upon the crystal lattice and their involvement into the local reduction mechanism. In Figs. 6(a)–6(c), we have interrupted the experiment before it reaches half of the cell. If we let the growth go on, we observe a morphological change around 50%, as shown in Fig. 6(e). The sodium ions migrate like the zinc ions from the anode towards the cathode but, in contrast to the later ones, they cannot be renewed during the experiment. As a consequence the growth meets, at some critical percentage of its development $\tau_c = \mu_{an}/(\mu_{an}+\mu_{sod})$ (~ 0.6 with standard table values), a zone which no longer contains any sodium ions and a transition from the former dense structure to a more dendritic one occurs. This transition, like the basic front transition discussed in the preceding section, scales with the total distance between cathode and anode, in other words, it always appears at the same percentage of the whole cell length, whatever the current density and the concentration of the metal cations. Taking different cations, as in Figs. 6(d)–6(f), one can even deduce from the position of their respective morphological transitions a rough estimate of their ionic mobilities [30]. It is worth noting that these transitions are also clearly visible in the temporal evolution of the cell potential. Since alkali metal ions are very common impurities (from a bad working ion exchange water supply, for example) we suggest that some of the transitions observed in the past could be explained this way. At least for experiments as in Ref. [21], where pH indicator salts have been purposely added to the solution, one must be aware of the unescapable presence of alkali metal cations and therefore of the appearance of additional transitions.

This type of impurities can also be imported in the system by the metallic wires which play the role of cathode and anode. Working with colored pH indicators, we have noticed a slight change of color after the injection of the electrolyte in the vicinity of both electrodes; which indicates a basification of this region, even without applied current, due to the protective hydroxide layer always present on zinc wire. By injecting the liquid with the help of a syringe these superficial impurities can indeed be mechanically removed from the wire and distributed inhomogeneously inside the cell by the filling procedure. Wherever the deposit looks denser, we know that the concentration of impurities is higher and we can even guess how the cell has been filled, from the simple observation of the morphological transition. In Figs. 7(b) and 7(c), we prepare two cells the same way but in experiment (b) the liquid is injected from both sides, whereas in run (c) it is injected from the right side only. The difference is clearly visible and the morphological changes are explained the following way: at first, the deposit grows in a solution polluted by the superficial impurities of the electrode, but these impurities are not renewed by the anodic process. When this "fresh" electrolyte meets the outgrowing pattern, a less dense structure continues to grow. In Fig. 7(b), we observe that the symmetric injection of the electrolyte leads to a symmetric pattern for the Hecker transition, and we can also add that this procedure gives a higher impurity concentration on the sides of the cell where the morphological transition is more noticeable. In Fig. 7(c), the cell was filled from the right side only and the Hecker transition reveals the contour of the fluid during the filling because the current has been

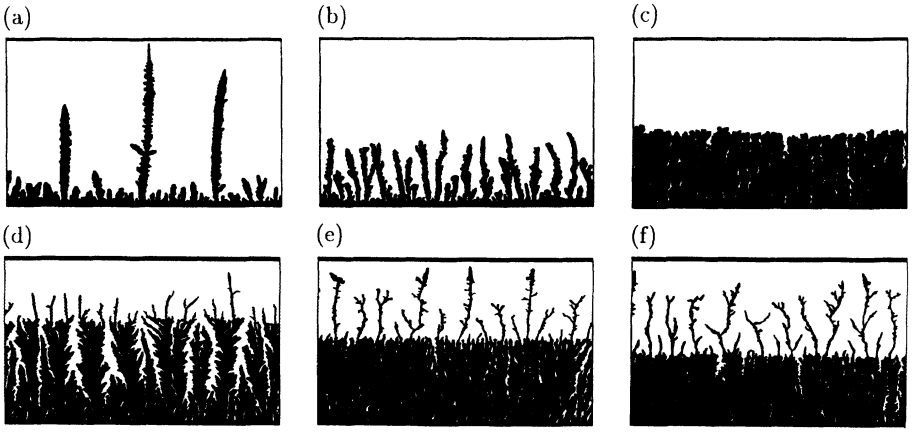

FIG. 6. The influence of alkali metal ions on the growth morphology. $[ZnSO_4]=0.1M$, $j=60$ mA cm^{-1}: (a) without sodium ions; (b) $1.25\times10^{-4}M$ sodium sulfate; (c) 1.25×10^{-3} sodium sulfate. Alkali metal ion transition: $[ZnSO_4]=0.05M$, $j=20$ mA cm^{-1}; (d) $2.5\times10^{-4}M$ lithium sulfate; (e) $2.5\times10^{-4}M$ sodium sulfate; (f) $2.5\times10^{-4}M$ potassium sulfate. The geometrical characteristics of the cell are $L=2$ cm, $W=5$ cm, $D=0.25$ mm.

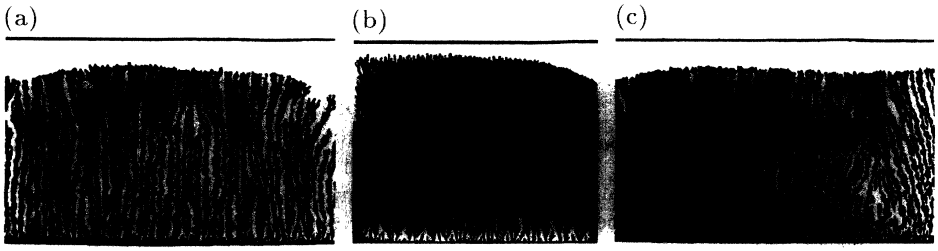

FIG. 7. Transition due to superficial electrode impurities, $[ZnSO_4] = 0.03M$, $j = 60$ mA cm^{-1}, $r = [H_2O_2]/[ZnSO_4] = 0.1$. (a) The cell has been rinsed, prior to use, by the zinc sulfate solution; (b) the liquid has been injected from both sides without rinsing the cell; (c) the liquid has been injected from the right side without rinsing the cell.

switched on immediately after it, without letting the electrolyte homogenize by diffusion. From the respective mobilities of the cationic impurities and of the anion, the type of polluting species which are the cause of this transition could be guessed. Rinsing the whole cell with an excess of electrolyte, prior to experiment, completely eliminates this kind of transition because all the superficial impurities are washed out of the cell, as in Fig. 7(a). In contrast to the previous transitions this one is less spectacular because the number of outgrowing branches does not change very much and this is the reason why it can hardly be observed in the evolution of the cell voltage. To conclude, we should mention that this effect can also be observed with different metals such as copper and it is probably the cause of most of the pattern inhomogeneities which can be recognized when revisiting the thin-layer electrodeposition literature.

C. Third transition: convective roll transition

It remains to explain a last transition which appears only very late in the experiment, when the growth has reached 80–90 % of the cell. In the case of pure dendritic morphologies, this transition is hardly perceptible, while in the case of dense patterns it corresponds to a clear slowing down or a stopping of the growth. As already suggested in the first section, the reasons for this behavior are convective rolls in front of both the anode and the cathode which result from strong local concentration gradients. We monitor the evolution of this concentration profile by dividing the cell into equidistant sections, after stopping the growth once it has reached a specific percentage of the cell. The zinc ion content of the liquid of every section is analyzed by standard analytical technique [ethylenediamine tetra-acetic acid (EDTA) titration]. The evolution of the zinc cation concentration profile with time is shown in Fig. 8. As time evolves, we observe a quick diminution of the zinc sulfate concentration in the vicinity of the cathode, whereas the anodic concentration is increased. These strong concentration gradients which are building up in front of the electrodes are going to couple with the gravity field to trigger convective motion (rolls), at the anode and the cathode, whose extent will depend on the depth of the fluid between the two glass plates and the applied current density [29]. Inside these rolls, the mixing is enhanced and in front of the anode, a zone where the zinc sulfate concentration is much greater than the bulk is created, as we have already noticed in Fig. 4(a) thanks to pH colored indicators. When the growth front approaches the anode, the leading tips of the growth meet a nonsteady, convection homogenized, and higher concentrated zinc sulfate solution. For typical values of depth and current density found in the literature, this happens around 80–90% of the cell length. The morphology is suddenly getting very compact, quasitridimensional because the depleted layer which makes the texture of the deposit ramified and tenuous is destroyed by the anodic roll. This is easier to detect in dense morphologies than in dendritic growth. Owing to the fact that the number of branches is greater, one cannot only observe the darkening of the texture [Fig. 1(e) or 1(f)], but also measure the slowing down of the growth.

This analysis gives a few indications that transport

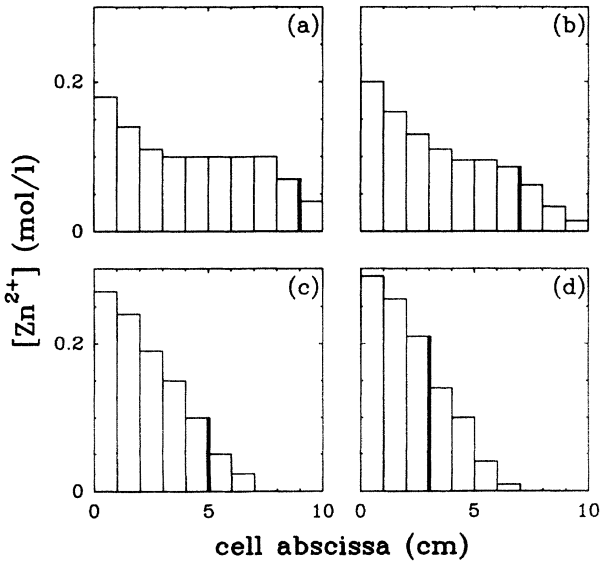

FIG. 8. Zinc sulfate concentration profiles measured by microsamplings at different stages of the growth, $[ZnSO_4] = 0.1M$, $j = 100$ mA cm^{-1}. Characteristics of the cell: $L = 10$ cm, $W = 8$ cm, $D = 1$ mm. The position of the growth is symbolized by a black vertical bar. (a) $t \sim 4$ min, 45 s; (b) $t \sim 10$ min; (c) $t \sim 21$ min; (d) $t \sim 41$ min. The anode and cathode positions are, respectively, 0 and 10 cm.

(diffusion, migration, convection) and reaction processes are deeply interacting in an interfacial process. The peculiar advantage of a growth experiment lies in the fact that the final pattern memorizes the whole past evolution and therefore the simple investigation of the texture of an electrodeposition pattern can inform us about the preponderant processes which have been working for its edification. Thin-layer electrodeposition could in particular be used as a qualitative but sensitive method for testing the chemical purity of electrolytic solutions.

IV. CONCLUSION

We have confirmed that in thin-layer electrodeposition of metals, the growth morphology is very sensitive to even small chemical perturbations. A change of the *p*H, the presence of small amounts of oxygen, minute quantities of alkali metal ions, and superficial impurities of the electrodes have been shown to be the cause of most morphological transitions observed in the past. The percentage of growth evolution where they occur depends very generally on the ratio of the mobility of the impurity over the mobility of the preponderant anion. We have observed a different type of transition (third type) which is induced by natural convection around the neighborhood of the electrodes. We should emphasize here that all the transitions disappear when working in an open reactor [24], which is continuously fed by a three-dimensional reservoir and where the anode is located externally to the thin layer of electrolyte. In this case, the transitions which are linked to the finite length of the cell (progressive depletion of the impurities which are mixed all over the cell at the beginning of the experiment or buoyancy convective instability at the anode) no longer exist. As already mentioned in a previous [22] publication, even in the case of steadily fed cells there could still remain morphological changes. We believe that they could be similar to the "impurity transition" that has been discussed at the end of Sec. III B, because this type of transition relies on a local pollution of the electrolyte by an air-spoiled metallic wire.

To conclude, let us emphasize the absolute necessity of checking the purity of the (supporting) electrolyte as well as the cell preparation to avoid any spurious and unexpected perturbation of the growth morphology.

ACKNOWLEDGMENTS

We are very grateful to A. Arneodo and J. Huth for useful discussions. This work has been supported by the Centre National des Etudes Spatiales under Contract No. 92/CNES/0225, NATO under grant No. RG 900685, and the DRET under Grant No. 89/196. The work of A.K. was supported by CEC under Contract No. S/SC1*/915114.

[1] *Growth and Form, Nonlinear Aspects,* Vol. 276 of *NATO Advanced Study Institute, Series B: Physics,* edited by M. Ben Amar, P. Pelcé, and P. Tabeling (Plenum, New York, 1991).

[2] T. Vicsek, *Fractal Growth Phenomena* (World Scientific, Singapore, 1992), and references therein.

[3] P. G. Saffman and G. Taylor, Proc. R. Soc. London, Ser. A **245**, 312 (1958).

[4] P. Tabeling and A. Libchaber, Phys. Rev. A **33**, 794 (1986).

[5] Y. Couder, N. Gerard, and M. Rabaud, Phys. Rev. A **34**, 5175 (1986).

[6] L. Niemeyer, L. Pietronero, and H. J. Wiesmann, Phys. Rev. Lett. **52**, 1033 (1984).

[7] H. Fujikawa and M. Matsushita, J. Phys. Soc. Jpn. **58**, 3875 (1989).

[8] S. C. Huang and M. E. Glicksman, Acta Metall. **29**, 717 (1984).

[9] J. S. Langer, Rev. Mod. Phys. **52**, 1 (1980).

[10] R. M. Brady and R. C. Ball, Nature (London) **309**, 225 (1984).

[11] R. Winand, Hydrometallurgy **29**, 567 (1992).

[12] F. Argoul, A. Arneodo, G. Grasseau, and H. L. Swinney, Phys. Rev. Lett. **61**, 2558 (1988).

[13] F. Argoul, A. Arneodo, J. Elezgaray, G. Grasseau, and R. Murenzi, Phys. Lett. A **135**, 327 (1989); Phys. Rev. A **41**, 5537 (1990).

[14] M. Matsushita, M. Sano, Y. Hayakawa, H. Honjo, and Y. Sawada, Phys. Rev. Lett. **53**, 286 (1984).

[15] Y. Sawada, A. Dougherty, and J. P. Gollub, Phys. Rev. Lett. **56**, 1260 (1986).

[16] D. Grier, E. Ben-Jacob, R. Clarke, and L. M. Sander, Phys. Rev. Lett. **56**, 1264 (1986).

[17] L. M. Sander, in *The Physics of Structure Formation* (Springer-Verlag, Berlin, 1987), p. 257.

[18] N. Hecker, D. G. Grier, and L. M. Sander, in *Fractal Aspects of Materials,* edited by R. B. Laibowitz, B. B. Mandelbrot, and D. E. Passoja (Materials Research Society, University Park, PA, 1985).

[19] P. Garik, D. Barkey, E. Ben-Jacob, E. Bochner, N. Broxholm, B. Miller, B. Orr, and R. Zamir, Phys. Rev. Lett. **62**, 2703 (1989).

[20] V. Fleury, M. Rosso, and J. N. Chazalviel, Phys. Rev. A **43**, 6908 (1991).

[21] J. R. Melrose, D. B. Hibbert, and R. C. Ball, Phys. Rev. Lett. **65**, 3009 (1990).

[22] P. P. Trigueros, J. Claret, F. Mas, and F. Sagues, J. Electroanal. Chem. **328**, 165 (1992).

[23] E. Ben-Jacob, G. Deutscher, P. Garik, N. D. Goldenfeld, and Y. Lareah, Phys. Rev. Lett. **57**, 1903 (1986).

[24] F. Argoul and A. Kuhn, J. Electroanal. Chem. **359**, 81 (1993).

[25] V. Fleury, J. N. Chazalviel, M. Ross, and B. Sapoval, J. Electroanal. Chem. **290**, 249 (1990).

[26] A. Kuhn and F. Argoul, J. Electroanal. Chem. (to be published).

[27] L. Antropov, *Electrochimie Théorique* (Mir, Moscow, 1975).

[28] J. St. Pierre and D. L. Piron, J. Electrochem. Soc. **137**, 2491 (1990).

[29] J. Huth, W. B. McCormick, H. L. Swinney, F. Argoul, and A. Kuhn (unpublished).

[30] A. Kuhn and F. Argoul, J. Chem. Educ. (to be published).

[31] A. Kuhn and F. Argoul, Fractals **1**, 451 (1993).

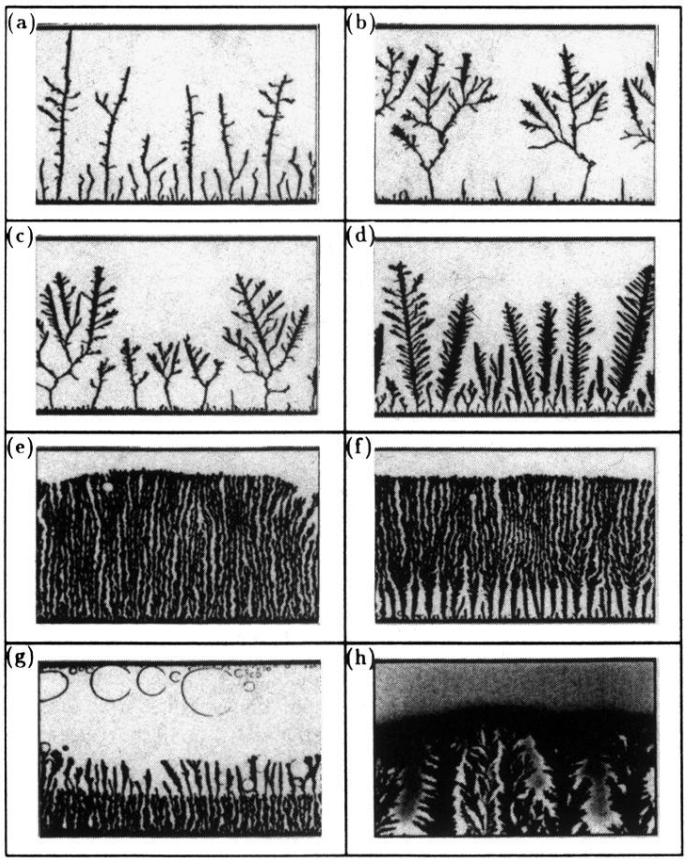

FIG. 1. Influence of the oxygen content and the acidity on the first morphological transition in thin-layer electrodeposition of zinc. The geometrical characteristics of the cell are width $W=5$ cm, length $L=2$ cm, and depth $D=0.25$ mm. The electrolyte is, except when otherwise mentioned, a $0.03M$ solution of $ZnSO_4$ with its normal pH and the current density is adjusted to 20 mA cm^{-2}. (a) The electrolyte has been purified by bubbling nitrogen through it for one hour; (b) without nitrogen purification; (c) after nitrogen purification, a proportion $r=[H_2O_2]/[ZnSO_4]=0.015$ of hydrogen peroxide has been added; (d) same as (c) with $r=0.02$; (e) same as (c) with $r=0.1$; (f) same as (e) with a pH adjustment to 2.7 by addition of sulfuric acid; (g) we have replaced the zinc anode by a silver anode, $r=0.1$, $[ZnSO_4]=0.03M$, and the current density j has been increased to 60 mA cm^{-2} to minimize the convective perturbation of the growth by the bubbles which are produced at the anode; (h) same as (f) with a few drops of pH indicator bromocresolpurple ($pK_a=6$): enlargement of the tips after the transition; the darker zone corresponds to the purple (basic) color of the indicator.

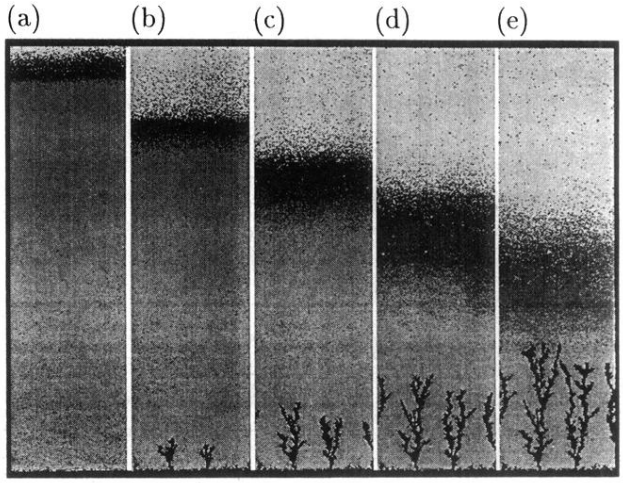

FIG. 3. Detection of the basic front with *p*H indicator bromocresolgreen ($pK_a = 4.6$), $[ZnSO_4] = 0.1M$, $j = 60$ mA/cm^2, the *p*H has been adjusted to 3.2 by the addition of sulfuric acid. The distance L between anode and cathode is 5 cm. (a) $t = 40$ s; (b) $t = 120$ s; (c) $t = 200$ s; (d) $t = 280$ s; (e) $t = 360$ s. Let us remark that as the growth evolves, the initial dark front which emerges from the anode (a) is getting wider and wider by diffusion process.

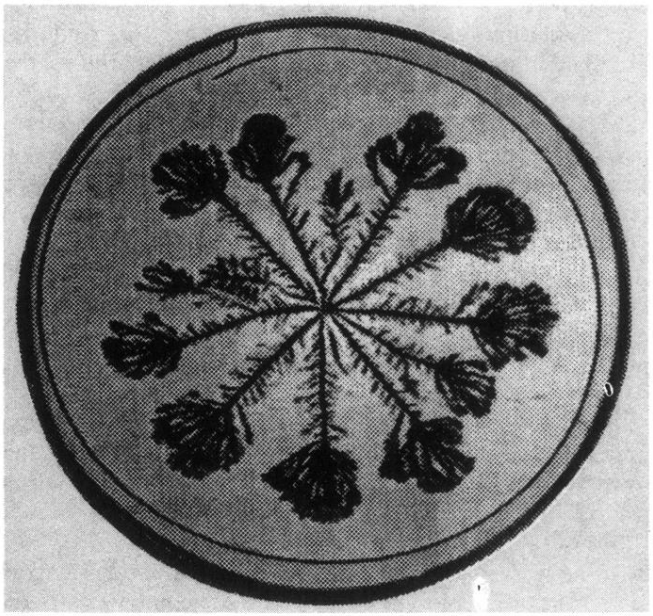

FIG. 5. The basic front transition in circular geometry. The diameter of the cell is 10 cm and its depth is 0.05 mm, $[ZnSO_4]=0.05M$, $r=[H_2O_2]/[ZnSO_4]=0.015$, $p\mathrm{H}=2.7$. The experiment is run under potentiostatic conditions with a global voltage $U=5$ V.

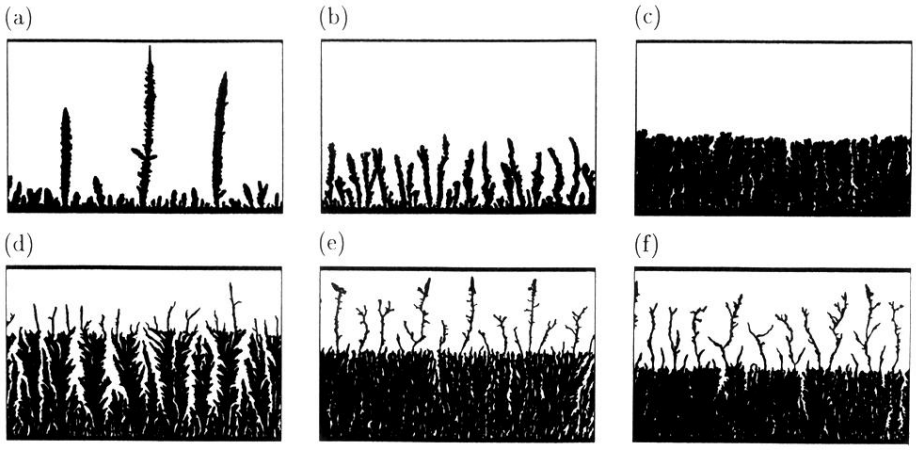

FIG. 6. The influence of alkali metal ions on the growth morphology. $[ZnSO_4]=0.1M$, $j=60$ mA cm^{-1}: (a) without sodium ions; (b) $1.25\times10^{-4}M$ sodium sulfate; (c) 1.25×10^{-3} sodium sulfate. Alkali metal ion transition: $[ZnSO_4]=0.05M$, $j=20$ mA cm^{-1}; (d) $2.5\times10^{-4}M$ lithium sulfate; (e) $2.5\times10^{-4}M$ sodium sulfate; (f) $2.5\times10^{-4}M$ potassium sulfate. The geometrical characteristics of the cell are $L=2$ cm, $W=5$ cm, $D=0.25$ mm.

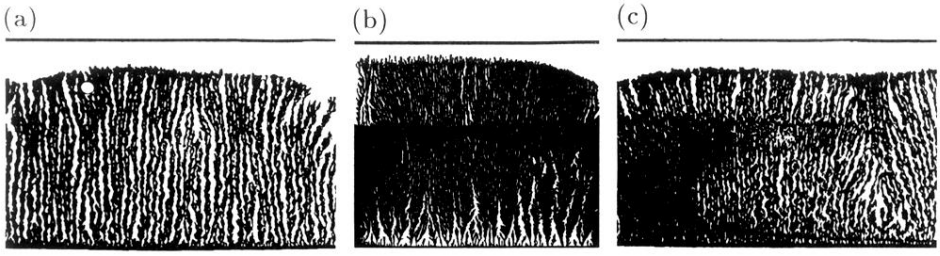

FIG. 7. Transition due to superficial electrode impurities, $[ZnSO_4] = 0.03M$, $j = 60$ mA cm^{-1}, $r = [H_2O_2]/[ZnSO_4] = 0.1$. (a) The cell has been rinsed, prior to use, by the zinc sulfate solution; (b) the liquid has been injected from both sides without rinsing the cell; (c) the liquid has been injected from the right side without rinsing the cell.